HAL
open science

Effects of solvent vapor annealing on the crystallinity and spin crossover properties of thin films of [Fe(HB(tz)3)2]

Alin-Ciprian Bas, Victoria Shalabaeva, Xavier Thompson, Laure Vendier, Lionel Salmon, Christophe Thibault, Gábor Molnár, Lucie Routaboul, Azzedine Bousseksou

To cite this version:

Alin-Ciprian Bas, Victoria Shalabaeva, Xavier Thompson, Laure Vendier, Lionel Salmon, et al.. Effects of solvent vapor annealing on the crystallinity and spin crossover properties of thin films of [Fe(HB(tz)3)2]. Comptes Rendus. Chimie, 2019, 22 (6-7), pp.525-533. 10.1016/j.crci.2019.03.002 . hal-02338991

HAL Id: hal-02338991

https://hal.science/hal-02338991v1

Submitted on 23 Nov 2020

HAL is a multi-disciplinary open access archive for the deposit and dissemination of scientific research documents, whether they are published or not. The documents may come from teaching and research institutions in France or abroad, or from public or private research centers.

L'archive ouverte pluridisciplinaire **HAL**, est destinée au dépôt et à la diffusion de documents scientifiques de niveau recherche, publiés ou non, émanant des établissements d'enseignement et de recherche français ou étrangers, des laboratoires publics ou privés.

Effects of solvent vapor annealing on the crystallinity and spin crossover properties of thin films of $[Fe(HB(tz)_3)_2]$

Effets d'un recuit en présence de vapeurs de solvant sur la cristallinité et les propriétés de transition de spin d'un film mince de [Fe(HB(tz)3)2].

Alin-Ciprian Bas,[a,b] Victoria Shalabaeva,[a] Xavier Thompson,[a] Laure Vendier,[a] Lionel Salmon,[a] Christophe Thibault,[b] Gábor Molnár,[a] Lucie Routaboul,[a*] and Azzedine Bousseksou[a*]

[a]LCC-CNRS, Université de Toulouse, CNRS, 31077 Toulouse, France.

[b]LAAS-CNRS, Université de Toulouse, CNRS, INSA, 31077 Toulouse, France

[*]Corresponding authors: lucie.routaboul@lcc-toulouse.fr, azzedine.bousseksou@lcc-toulouse.fr

Abstract. We investigated the solvent vapor annealing process of thermally evaporated thin films of the $[Fe^{II}(HB(tz)_3)_2]$ (tz = 1,2,4-triazol-1-yl) spin crossover complex. Using grazing incidence X-ray diffraction, atomic force microscopy and variable-temperature UV spectrophotometry, we show how the crystallinity, morphology and spin crossover properties of the resulting films are altered by exposure to vapors of five different solvents: diethyl ether, acetone, dichloromethane, ethanol and water. Remarkably, most solvents yielded highly oriented crystalline films displaying an abrupt and complete spin transition around 336 K. A notable exception is the case of dichloromethane - suggesting that the solvent ability to accept hydrogen bonding might be a key factor in controlling the film crystallinity. On the other hand, only water vapor treatment affords for smooth and continuous film morphology. The recrystallization process in controlled humidity was thus followed *in situ* by monitoring the UV absorbance of the films. This study revealed the critical importance of the relative humidity (RH): for values above a threshold of *ca.* 72 % RH (at 298 K) a very fast (seconds) crystallization occurs leading the robust, crystalline films, while

crystallization at lower RH values is slower (hours) and leads to less stable, semi-crystalline films displaying incomplete spin transitions.

Résumé. Nous avons étudié le recuit en présence de vapeurs de solvant d'un film mince obtenu par évaporation thermique du complexe à transition de spin $[Fe^{II}(HB(tz)_3)_2]$ (tz = 1,2,4-triazol-1-yl). L'utilisation de la diffraction des rayons X à angle rasant, de la microscopie à force atomique et de la spectrométrie UV à température variante nous a permis de montrer l'évolution de la cristallinité, de la morphologie et des propriétés de transition de spin de ces films minces après leurs expositions à différentes vapeurs de solvants (éther diéthylique, eau, acétone, dichlorométhane et éthanol). De façon remarquable, la majorité de ces solvants conduisent à des films cristallins (la cristallinité préférentiellement orientée) qui possèdent une transition de spin abrupte et complète à une température proche de 336K. Cette étude montre que le dichlorométhane est une exception notable ce qui suggère que la capacité du solvant à accepter les liaisons hydrogène pourrait être un facteur clé dans le contrôle de la cristallinité du film. Par ailleurs, seul le traitement en présence de vapeurs d'eau conduit à un film peu rugueux et de morphologie régulière. Le procédé de recristallisation sous humidité contrôlée a aussi été suivi in situ par la mesure de l'absorbance dans l'UV de ces films. Cette étude révèle que l'humidité relative (RH) est un critère primordial : pour des valeurs autour ou supérieures à 72% de RH (à T=298 K) une recristallisation très rapide (à l'échelle de la seconde) s'effectue et conduit à un film cristallin alors que la recristallisation réalisée avec des valeurs de RH plus basses mène à des films semi-cristallins qui sont moins stables et qui possèdent une transition de spin incomplète.

Keywords. Spin crossover complex, solvent vapor annealing, thin films, crystallinity, UV/Vis spectroscopy, X-ray diffraction.

Mots Clés. Complexe à transition de spin, effets de vapeurs de solvant, films minces, cristallinité, spectroscopie UV/Vis, diffraction des rayons X.

Introduction

Spin crossover (SCO) complexes exhibiting a reversible switching between their low-spin (LS) and high-spin (HS) electronic configurations have received considerable attention due to their fascinating ability to change magnetic, optical, electrical and mechanical properties as a response to different external stimuli such as changes of temperature, pressure, magnetic field and others.[1–4] Thanks to the recent progress in nanoscale organization of SCO compounds into films and nanoparticles, SCO materials have become very attractive for their implementation in nanosized devices for electronic, spintronic, photonic and nanomechanical applications.[2,5–9]

In this context, we have recently been extensively investigating the molecular spin crossover compound $[Fe^{II}(HB(tz)_3)_2]$ (tz = 1,2,4-triazol-1-yl) **(1)**.[10] It is characterized by an isostructural and abrupt first-order spin transition between its LS and HS configurations, near room temperature (*ca.* 333 K), with a narrow thermal hysteresis loop (*ca.* 2 K width).[11] An optical microscopy study of the nucleation-growth dynamics of the spin transition in single crystals of **(1)** demonstrated exceptionally fast switching kinetics and a remarkable mechanical resilience upon repeated thermally induced spin transition.[12] Moreover, compound **(1)** was used to synthesize high-quality thin films by thermal evaporation under high vacuum conditions, providing films with a very high purity and tight thickness control.[13] This allowed us to investigate, in detail, the thickness dependence of the spin transition in the films.[14] The ability to feature continuous thin films, whose thickness can be tuned with nanometric precision, in combination with the spin transition just above room temperature, makes compound **(1)** very attractive for the implementation in nanoscale devices. Notably, crystalline thin films of **(1)** were integrated into micro-electromechanical systems (MEMS) in which the SCO molecules were used to tune the device mechanical properties and to perform controlled and reversible macroscopic work.[15,16] We also succeeded in fabricating large-area crossbar electrical junctions from thin films of **(1),** in which we observed resistance switching upon the SCO.[17] Then, using liquid electrodes, a higher magnitude resistance switching was demonstrated by Poggini *et al.* in tunneling junctions of **(1)**.[18]

It is important to stress that pristine, thermally evaporated thin films of $[Fe(HB(tz)_3)_2]$ usually show poor environmental stability and stable, reproducible films could be obtained only by post-deposition annealing. Indeed, the crystalline structure, morphology and SCO properties of freshly deposited films significantly alter over time in ambient air, making them difficult to integrate as building blocks in nanodevices. To overcome this problem, we previously demonstrated that thin

films of **(1)** with extremely robust SCO properties could be obtained by means of a simple solvent vapor annealing (SVA) process. Notably, the exposure of the freshly evaporated amorphous films to water vapor (*ca.* 75–80 % relative humidity, RH) at room temperature led to very efficient and fast crystallization.[13] These crystalline films turned out to be remarkably stable in ambient air for long periods and over (at least) four SCO cycles.

In the present study, we systematically examined the crystallinity, morphology and SCO characteristics of thin films of **(1)** after their exposure to the vapors of five different solvents: diethyl ether, acetone, dichloromethane, ethanol and water. $[Fe(HB(tz)_3)_2]$ films were characterized by means of grazing incidence X-ray diffraction (GIXRD), atomic force microscopy (AFM) and variable-temperature ultraviolet-visible (UV-Vis) absorption techniques. The crystallization process upon water exposure was further investigated by *in-situ* absorbance measurements using a dedicated environmental chamber with simultaneous humidity and temperature control.

Experimental

Reagents and solvents used in this study are commercially available. The bulk powder of **(1)** was synthesized as described in ref. 11. Thin films with thicknesses in the 100 - 200 nm range were grown by thermal evaporation in a PREVAC film deposition system at a base pressure of *ca.* 2×10^{-7} mbar. The bulk powder was heated until 250 °C in a quartz crucible and evaporated at a rate of 0.03 Å s^{-1}. The evaporation rate and film thickness were monitored *in situ* using a quartz crystal microbalance. The final film thickness was determined using AFM. The films were deposited onto fused silica substrates, which were cleaned with acetone and isopropanol to remove contaminants. For solvent vapor annealing, we used five different solvents: diethyl ether, acetone, dichloromethane, ethanol and water. After film deposition, the substrates with $[Fe(HB(tz)_3)_2]$ thin films were immediately placed in a sealed vial of 60 ml along with an open vial containing 10 ml of a given solvent. This led to a saturated solvent atmosphere in the large vial while direct contact between the film and the liquid was avoided. Except otherwise stated, annealing was carried out at room temperature for 10 min. Identical vials were used for each experiment thus leading to different saturated vapor pressures for the different solvents.

The GIXRD experiments were carried out in a PANalytical X'Pert PRO MPD system using Cu-Kα radiation (45 kV and 40 mA) with a parallel-beam configuration. The incident beam optics consisted of a mirror with a 1/32° divergence slit. A parallel plate collimator (0.18°) and Soller

slits (0.04°) were mounted on the path of the diffracted beam. An X'Celerator detector in receiving slit mode was used for X-ray collection. AFM surface topography measurements were done using a Cypher-ES microscope (Oxford Instruments) in amplitude-modulation mode, in ambient air using OMCLAC160TS-R3 (Olympus) probes. Optical microscopy images were acquired in reflectivity mode using a Motic stereomicroscope equipped with a digital camera. The temperature dependent absorbance spectra of the thin films were collected at wavelengths between 250 and 800 nm using a Cary 50 (Agilent Technologies) spectrophotometer and a Linkam FTIR-600 heating-cooling stage, equipped with fused silica windows. The sample chamber was purged with dry nitrogen and spectra were acquired in the 293–393 K range with 1 K min^{-1} rate. For *in-situ* absorbance measurements, the heating-cooling stage was connected to a Linkam RH95 humidity controller, which allows for a fine control of the humidity around the sample between 5 and 90 % RH.

Results and discussion

SVA, which consists of exposing a film to a solvent vapor at (or near) room temperature, has recently become an increasingly popular 'mild' method to control thin film morphology and crystallinity. Considering that one can use various solvents with different solubility parameters and vapor pressure, SVA represents a highly versatile approach. In particular, the effects of solvent vapors on block copolymer films,[19–22] organic semiconductors films[23–27] and compounds of pharmaceutical interest[28,29] have been described formerly. However, the effects of solvent vapors on SCO films were previously not much explored.[13,30] The effects of SVA mainly depend on the properties of applied solvents.[23,24,26] Solvent molecules interact with the surface of a material and, depending on solvent-material affinity, film permeability, morphology, exposure time and temperature, the solvent can diffuse into it or condense on the surface and dissolve molecules. In either case, the 'softening' of the material then enables movement and/or rearrangement of molecules.

The solubility of **(1)** is rather low in common solvents. Among those used in this study, diethyl ether, acetone and ethanol can be considered as non-solvents, while water and dichloromethane are "poor solvents" (*ca.* 1 mg/mL at 298 K). We have chosen these solvents with different polarities, vapor pressures and hydrogen-bonding abilities to enable meaningful comparisons. Table 1 gathers some commonly used quantitative parameters describing these properties. In

particular, the Hansen solubility parameters characterize the cohesive energy density of the substance, decomposed for dispersive interactions (δ_d), polar interactions (δ_p) and hydrogen bonding contributions (δ_H). The vapor pressure (P_v), boiling point (T_b) and surface tension (γ) are also related to the cohesive forces between the solvent molecules, while the Gutmann donor number (*DN*) is used to quantify the Lewis basicity of solvents.

Table 1. Solvent properties[31]: Hansen solubility parameters (dispersive, polar and H-bonding) in units of MPa, vapor pressure (at 20 °C) in units of kPa, boiling point (at 1 atm) in units of °C, surface tension (at 20 °C in air) in units of mN/m and Gutmann donor numbers in units of kcal/mol.

Solvent	δ_d	δ_p	δ_H	P_v	T_b	γ	DN
Water	15.5	16.0	42.3	3.17	100	72.8	18
Ethanol	15.8	8.8	19.4	5.95	78.3	22.1	32
Diethyl ether	14.5	2.9	4.6	58.7	34.6	17.1	19.2
Dichloromethane	17.0	7.3	7.1	57.3	39.8	26.5	1
Acetone	15.5	10.4	7.0	30.6	56.3	25.2	17

First, we analyzed by GIXRD the crystalline structure of the five solvent-exposed [$Fe(HB(tz)_3)_2$] films of ca. 200 nm thickness. In the diffraction geometry used, only crystal planes parallel to the substrate can be observed. This allows probing the crystallinity (and crystal structure) and determination of the preferred crystal orientation. Fig. 1 shows the diffraction patterns of the solvent annealed films as well as that of the freshly evaporated film. One may notice that the initial featureless diffraction pattern of the amorphous, pristine film drastically changes after exposure to the different solvents. Remarkably, the diffraction pattern of each solvent annealed film is dominated by a single, intense and narrow peak at a 2θ value of 10.01°. We have previously reported this diffraction peak for the humidity annealed films and, by comparison with the XRD pattern of the bulk powder, we could unambiguously assign it to the *002* reflection.[13] This result denotes crystalline order and preferential orientation of the water-annealed film with the orthorhombic *c*-axis normal to the substrate (Scheme 1). Most likely, the films adopt this orientation because of the low surface energy of the *00l* planes. The key experimental finding of the present work is that water is not the only solvent, which recrystallizes the films. However, one may notice that the film treated with CH_2Cl_2 exhibits a significantly weaker diffraction intensity at 10.01° in comparison with the films exposed to other solvents. In addition, the XRD pattern of the dichloromethane-exposed film exhibits other diffraction peaks with relatively high intensities

(with respect to the main peak). These results denote that the crystallinity and ordering of the dichloromethane-annealed films is lower when compared to other samples.

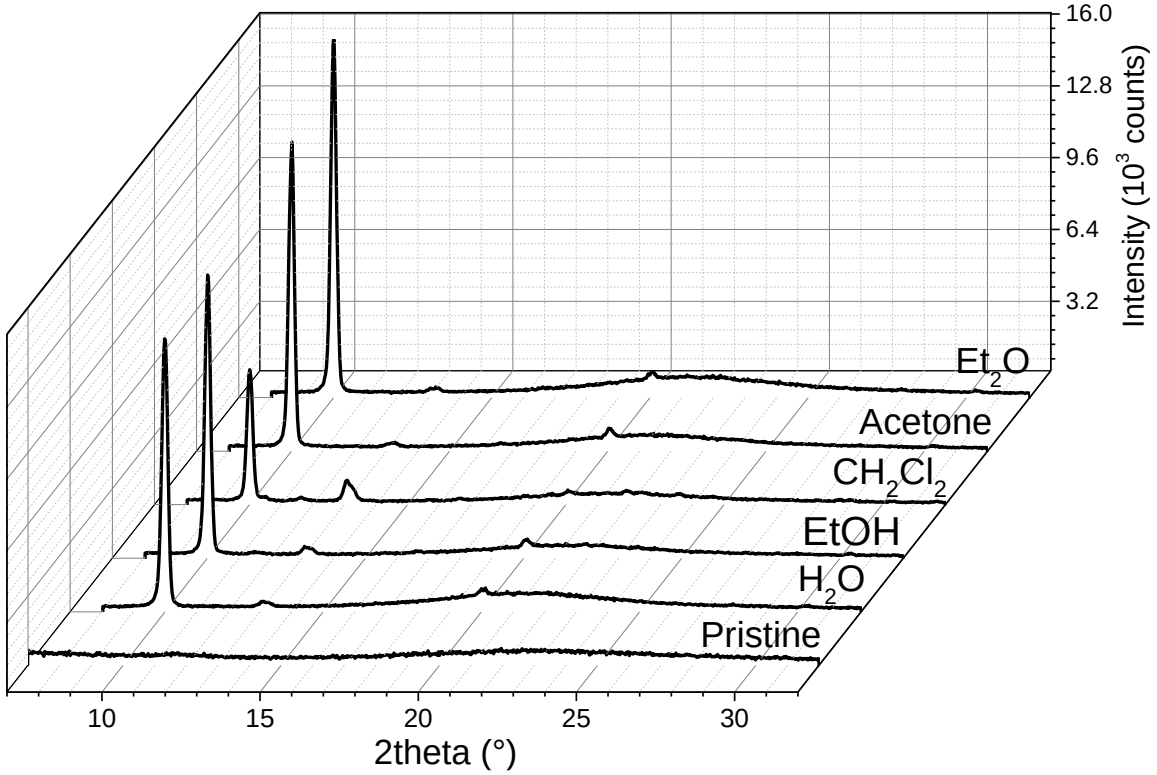

Figure 1. XRD patterns of $[Fe(HB(tz)_3)_2]$ thin films exposed to different solvents. The diffractogram of a pristine film is also shown. (*N.B.* The broad peak around 2θ = 15°–27° is typical for amorphous fused silica substrates used in this study.[32])

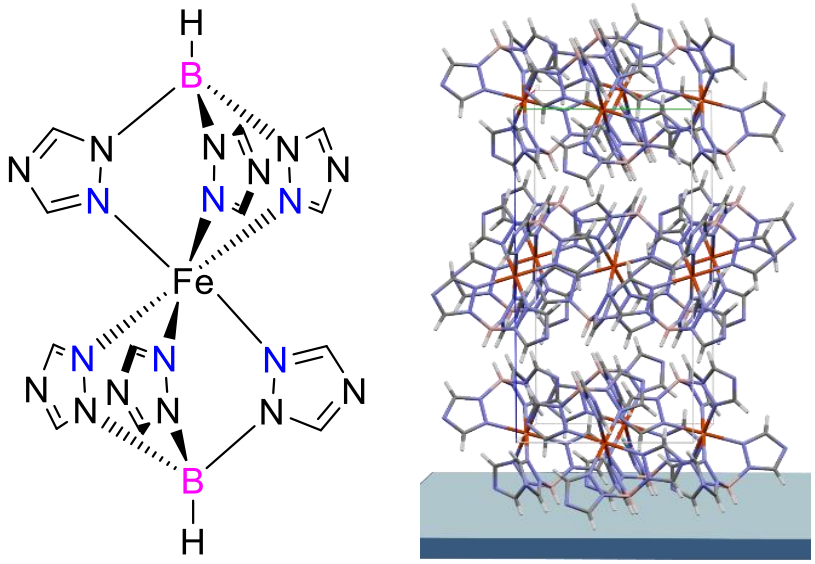

Scheme 1. (a) Molecular structure of $[Fe(HB(tz)_3)_2]$ and (b) its crystal structure in oriented thin films.

To investigate how the different crystallinity of the films alter the SCO properties, we performed variable temperature optical absorption measurements over two heating – cooling cycles between 293 K and 393 K. Fig. 2a shows selected UV absorbance spectra of the SCO thin films annealed with different solvents. The intense absorption bands between 260 and 340 nm are bleached upon increasing the temperature from 293 to 393 K, which can be explained by the SCO phenomenon. Fig. 2b displays the absorbance (at 318 nm) as a function of temperature for the different solvent-treated films. One may note that all films exhibit a rather abrupt spin transition with similar transition temperatures ($T_{1/2} \approx 336$ K) and small hysteresis widths ($\Delta T \approx 2$ K) (see also Table 2). However, the shape and intensity of the absorption spectra of the CH_2Cl_2-treated sample is different from the others and therefore the absorbance change upon the spin transition is drastically reduced in this sample indicating an incomplete SCO (*ca.* 36 %). In addition, the absorbance change between the LS and HS states (Abs_{LS}- Abs_{HS}) and intensity of the XRD peak at $2\theta = 10.01°$ (I_{002}) are correlated for the different samples (see Fig. 2c and Table 2). These findings suggest that the lower degree of crystallinity and ordering could be the primary cause for the very incomplete spin transition in the CH_2Cl_2 vapor annealed sample.

Table 2. Properties of solvent annealed films: spin transition temperature, hysteresis width, absorbance coefficient change upon the spin transition (at 318 nm), intensity of the *002* XRD peak (thickness normalized), UV-vis absorption coefficient at 400 nm (baseline corrected).

Solvent	$T_{1/2}$ (K)	ΔT (K)	α_{LS}-α_{HS} (10^4 cm^{-1})	I_{002} (counts)	Abs_{400nm} (baseline corrected)
Diethyl ether	335.6	1.6	2.85	13000	0.13
Acetone	336.0	1.3	2.97	13500	0.15
Dichloromethane	338.9	3.5	1.05	4740	1.23
Ethanol	335.7	3.1	2.92	12400	0.11
Water	336.0	2.2	2.74	12100	0.07

When comparing the properties of the different solvents used (see Table 1 and Fig. 2c), it appears that the poor crystallinity of the sample treated with dichloromethane and consequently its inferior SCO properties might be related to its low donor number, *i.e.* its low ability to accept hydrogen bonds, in comparison with the four other solvents used in our study. We can thus suggest that the SVA treatment of films of **(1)** is more efficient when the SCO molecules can form hydrogen bonds with the solvent molecules. Since **(1)** is much less soluble in diethyl ether/acetone/ethanol than in dichloromethane, the most plausible mechanism of SVA in the present case would be solvent diffusion into the film causing intermolecular hydrogen bonds to

break. Then, the higher mobility of the SCO molecules can allow the pristine metastable film to evolve into a thermodynamically more favorable crystalline state.

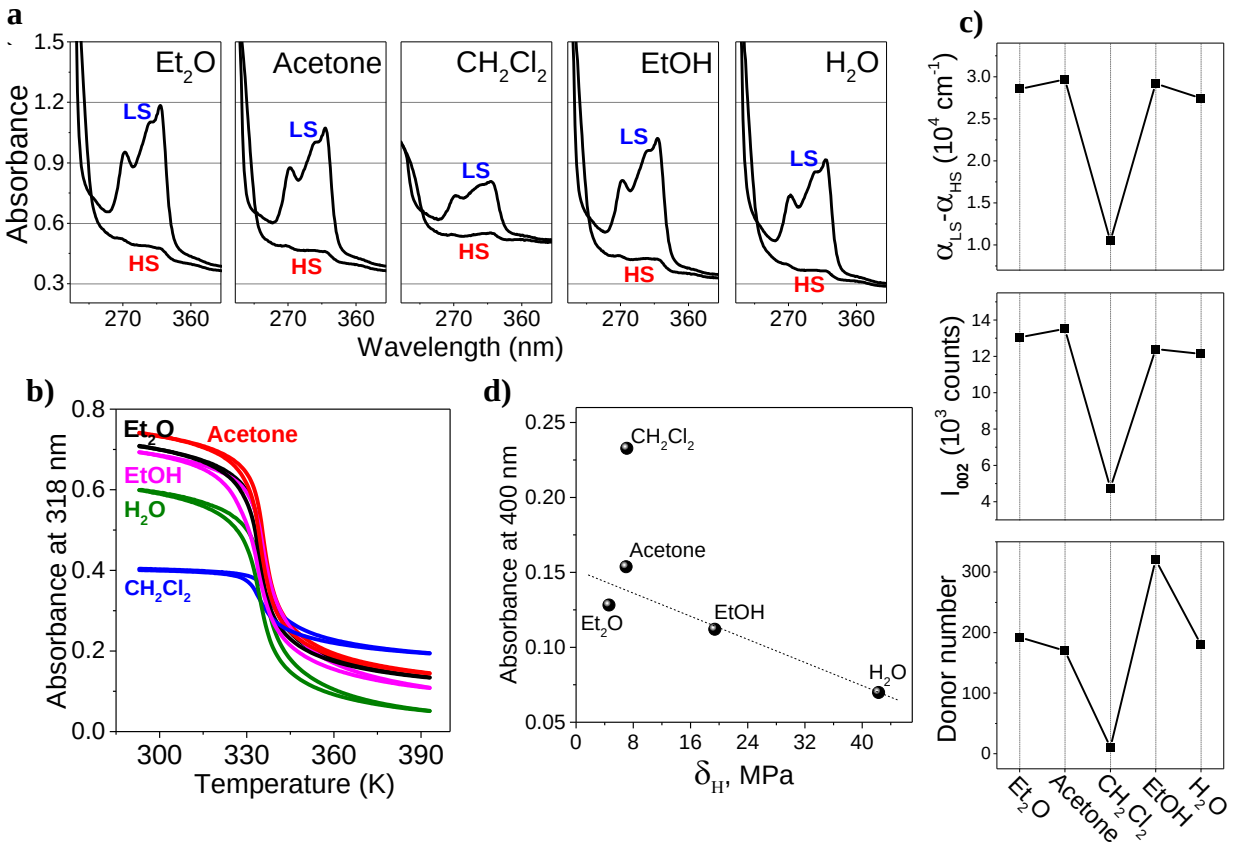

Figure 2. (a) Absorbance spectra acquired at 293 K (LS) and 393 K (HS) in the heating mode for $[Fe(HB(tz)_3)_2]$ films annealed with different solvents (uncorrected spectra). (b) Temperature dependence of the absorbance at 318 nm (baseline corrected) along the second heating–cooling cycle recorded at 1 K min^{-1} scan rate for different solvent treated samples. (c) Absorbance coefficient change at the spin transition (λ = 318 nm), intensity of the *002* XRD peak (thickness normalized) and solvent donor number for different solvent treated samples. (d) Absorbance at 400 nm (baseline corrected) as a function of the Hansen solubility parameter δ_H.

Another interesting observation one can make about the absorption spectra in Fig. 2a-b of the different solvent treated samples is their substantially different spectral baseline (see also Table 2). This finding denotes that the light scattering intensity of the films strongly differs, indicating that the morphology of the films must be different. To further investigate this aspect, we examined the surface morphology of different solvent-exposed $[Fe(HB(tz)_3)_2]$ films using optical microscopy and AFM. Fig. 3 shows the optical and AFM topography images of the thin films after exposure to the solvents. The water-exposed $[Fe(HB(tz)_3)_2]$ film is characterized by a smooth and continuous morphology, while the other samples appear more irregular. At first glance, the AFM topography images suggests that CH_2Cl_2 as well as EtOH treated films are smooth, characterized

by low values of arithmetic average roughness R_a. However, in this case the small area AFM topography analysis is not representative as optical images show the presence of some large-scale aggregates/crystals in these samples as well.

Interestingly, the light scattering intensity (i.e. the baseline of the absorbance spectra) is correlated with the Hansen solubility parameter δ_H of the solvents (Fig. 2d), denoting that the surface roughness decreases when δ_H increases. (*N.B.* The case of CH_2Cl_2 deviates from this trend, but we believe the deviation occurs due to its different crystallinity.) The solubility parameters of solvents have already been reported to be correlated with the changes in crystallinity and morphology of various organic films when exposed to the solvents.[23,24,28,29,33] In our case we can suggest that during SVA, water not only diffuses into the film as we suggested above for the different solvents, but for its lower vapor pressure, it may also condense on the surface of the pristine film. Since the solubility of **(1)** in water is not very high, fast supersaturation occurs and a large number of crystallization seeds form simultaneously, leading to densely packed, small crystallites and thus a smooth surface morphology. For the other solvents, larger crystals form, which indicates different film growth mechanism(s) involving possibly no surface condensation and less nucleation seeds.

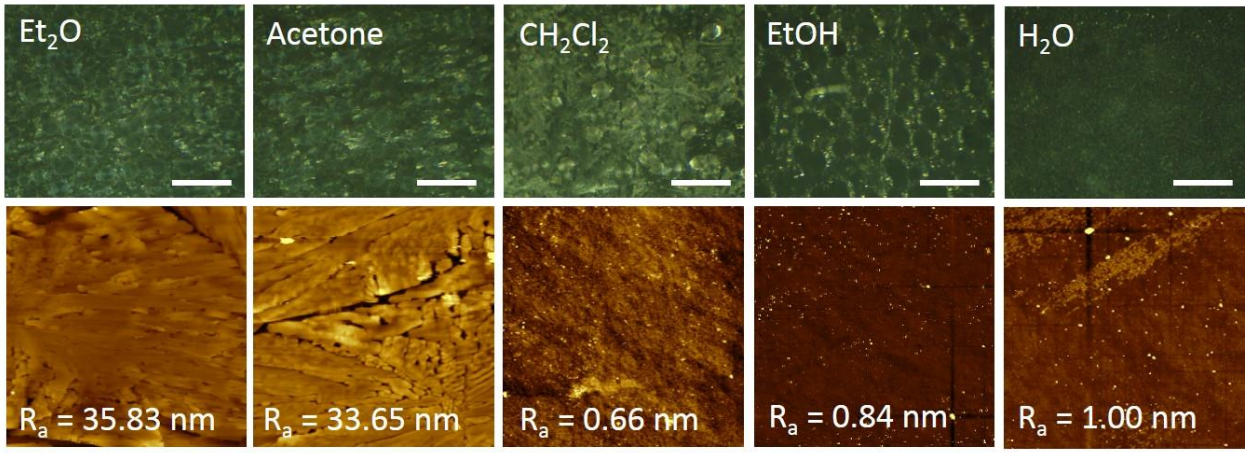

Figure 3. Optical microscopy (top panel) and AFM surface topography (bottom panel) characterization of the different solvent vapor annealed $[Fe(HB(tz)_3)_2]$ films. Scale bar in optical images: 500 µm; AFM image size: 30×30 µm^2.

Overall, we can conclude that the water vapor annealing gives the most efficient recrystallization procedure, offering the best control on film morphology, crystallinity and SCO properties. Driven by the aim to better understand the physical mechanisms of water vapor annealing process, we performed *in situ* UV-vis measurements with precise control of relative

humidity and temperature. (N.B. Due to the fast kinetics of the annealing process we were unable to conduct *in-situ* AFM and GIXRD measurements.) For *in-situ* spectroscopy, a freshly evaporated film of $[Fe(HB(tz)_3)_2]$ was placed in a temperature controlled chamber, wherein the relative humidity was changed from 40 to 80 % while measuring the absorbance of the film at a sampling rate of 10 Hz. Figure 4 displays the absorbance change at 318 nm together with the variation of RH for a fixed temperature of 298 K.

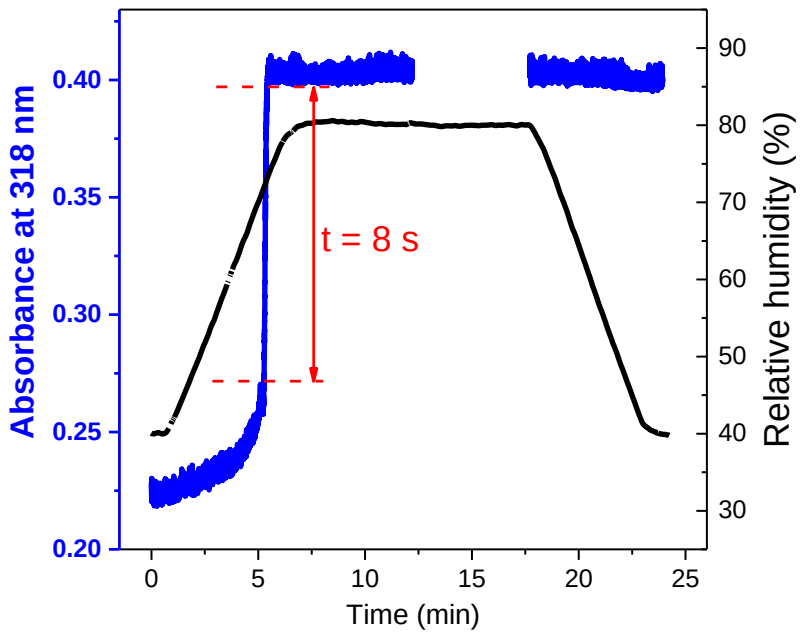

Figure 4. Absorbance change (baseline corrected) at 318 nm of a $[Fe(HB(tz)_3)_2]$ thin film as a function of time (blue curve) for increasing and decreasing values of relative humidity (black curve) at a fixed temperature of 298 K. (Note that between ca. 12.5 and 17.5 min no absorbance data were acquired.)

The striking observation here is the very abrupt change in absorbance at a relative humidity value of *ca.* 72 %. In a short period of *ca.* 8 s, the absorbance of the film increases sharply from 0.27 to 0.40. Before this increase the absorbance change is slow, while after the jump the absorbance of the film remains constant for any value of RH, *i.e.* the effect is irreversible. This result was repeatedly observed on fresh films and corroborates our hypothesis that the crystallization of the film during the water vapor annealing occurs by the simultaneous nucleation of a large number of seeds, which then form small, densely packed crystals. The crystalline state reached at the end of the process is extremely stable in air even for repeated thermal cycling. It is worth noting that the humidity treatment results in a solvated film, but the water molecules are

desorbed in ambient air *below* the spin transition temperature and they have therefore no effect on the SCO properties.[11,13]

Obviously, the water vapor annealing process is influenced by many parameters such as temperature, fluctuations of RH and exposure time. Regarding this last parameter, we observed that the films remain stable during longer exposure (2 h) to humidity, while the other solvent vapors led to the deterioration or even the complete dissolution (or dewetting) of the films. On the other hand, increasing the temperature of the substrate during the water vapor annealing led to decreasing efficiency. At 303 K, the crystallization was still observed, although more gradually. At higher temperatures, however, no absorbance change was detected even for RH 90% indicating less efficient interaction with the water molecules. Furthermore, we observed that keeping the films in ambient air before water vapor treatment leads to an irreversible evolution ('aging') of the films towards an ill-defined, semi-crystalline state. Figure 5a depicts the results of water vapor annealing of three similar films with *ca.* 100 nm thickness, which were beforehand stored in ambient humidity of *ca.* 57 % for 2 min, 15 min and 2.5 hours.

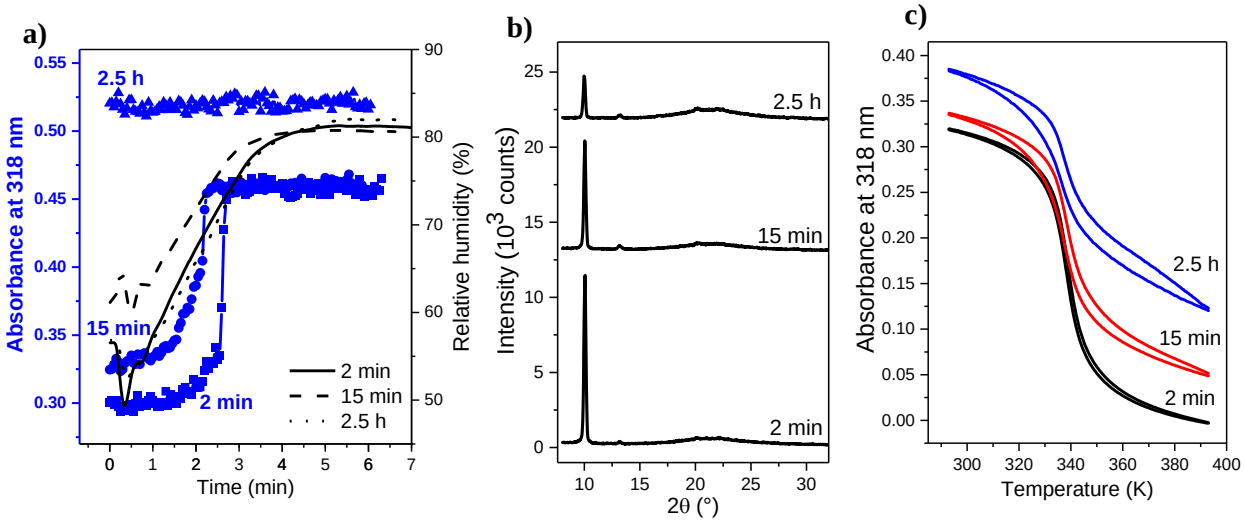

Figure 5. Investigation of three different $[Fe(HB(tz)_3)_2]$ thin films (each approx.. 100 nm thick) stored in air for 2 min, 15 min and 2.5 hours before water vapor annealing: (a) Absorbance change (λ = 318 nm; baseline corrected) during water vapor annealing (i.e. for increasing the RH from the ambient value to 80 %). (b) XRD patterns and (c) temperature dependence of the absorbance (second heating–cooling cycle, λ = 318 nm, dT/dt = 1 K min^{-1}; baseline corrected) following the water vapor treatment.

One can notice that the film exposed for 2.5 hours displayed a high initial absorbance and did not show any further increase of absorbance with increased relative humidity. This film then revealed different properties compared to the 'freshly treated' samples. Notably, the 10.01° XRD peak intensity of the film exposed to ambient air for 2.5 h is four times less than the peak intensity

of the film with only 2 min exposure to ambient air (see Fig. 5b and Table 3). In addition, the relative intensity of other diffraction peaks became more pronounced, indicating that in ambient air, the film evolves in an irreversible manner towards a less crystalline state and less oriented texture. In line with this observation, the spin transition became less complete and less abrupt for prolonged 'aging' in ambient air (Fig. 5c). In addition, the shape of the SCO curves displays an unusual hysteresis over the entire heating-cooling cycle, which indicates continuous sample evolution. We can thus conclude that water vapor annealing (RH > 72 %) applied to freshly evaporated $[Fe(HB(tz)_3)_2]$ films provides the best opportunity to achieve an abrupt and complete SCO transition with a high environmental stability, while the slow 'aging' of the films at lower relative humidity (i.e. in ambient air) leads to semi-crystalline films displaying, as a consequence, ill-reproducible, incomplete and broad spin transitions (see Scheme 2 for a summary of these phenomena).

Table 3. Properties of $[Fe(HB(tz)_3)_2]$ thin films stored in ambient air for different times before humidity treatment.

Aging time	$T_{1/2}$ (K)	ΔT (K)	Abs_{LS}-Abs_{HS}	I_{002} (counts)	Abs_{400nm} (baseline corrected)
2 min	339.2	0.9	0.32	11200	0.09
15 min	339.0	2.4	0.29	7200	0.14
2.5 h	339.5	3.8	0.26	2800	0.20

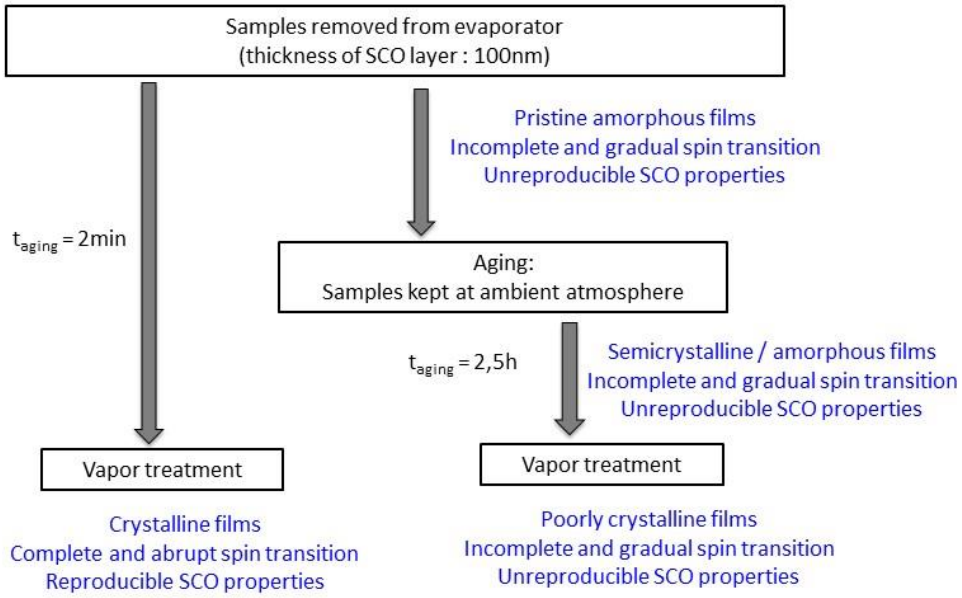

Scheme 2. Summary of the sample evolution depending on the experimental conditions.

Conclusions

[$Fe(HB(tz)_3)_2$] thermally evaporated thin films were recrystallized by means of solvent vapor annealing using five different solvents: diethyl ether, acetone, dichloromethane, ethanol and water. Grazing incidence X-ray diffraction and UV spectrophotometry showed that the EtO_2, $(CH_3)_2CO$, EtOH and H_2O treated films feature highly oriented crystalline structure and an abrupt spin transition at *ca.* 336 K. CH_2Cl_2 vapor annealed films are less crystalline and do not exhibit a complete spin transition. On the other hand, water appeared to be the only solvent, which provides a smooth and continuous film morphology. The recrystallization process in water was then studied by UV absorption measurements with *in situ* humidity control. This analysis showed that the crystallization is complete within a few seconds above a threshold humidity value. Based on these findings we suggested that the key parameters responsible for film crystallinity and for the control of film morphology could be the hydrogen bonding ability of the solvents as well as their solubility parameters. On the whole, solvent vapor annealing provides a simple and fast, yet very powerful method to control crystallinity, texture, morphology, spin crossover properties and environmental stability of thin films of [$Fe(HB(tz)_3)_2$], which is crucial for the integration in a broad range of nanosized devices. We believe this approach will be increasingly important for the engineering of various SCO films.

Acknowledgments. This work was supported by by the European Commission through the SPINSWITCH project (H2020-MSCA-RISE-2016, Grant Agreement No. 734322). The grants of AB, VS and XT were financed by the Région Occitanie (no. 15050123), the EMERGENCE@INC208 project and by the Louisiana State University LSAMP International Research Experience Project for Undergraduates (NSF Grant #1560390), respectively. The authors are grateful to Linkam Scientific Instruments for the loan of the RH95 humidity controller.

(1) Gütlich, P.; Goodwin, H. A. *Topics in Current Chemistry. Spin Crossover in Transition Metal Compounds*; Springer-Verlag: Berlin, 2004.

(2) Bousseksou, A.; Molnár, G.; Salmon, L.; Nicolazzi, W. Molecular Spin Crossover Phenomenon: Recent Achievements and Prospects. *Chem. Soc. Rev.* **2011**, *40* (6), 3313–3335.

(3) Halcrow, M. A. *Spin-Crossover Materials : Properties and Applications*; Wiley-Blackwell,

2013.

(4) Gütlich, P.; Hauser, A.; Spiering, H. Thermal and Optical Switching of Iron(II) Complexes. *Angew. Chemie Int. Ed. English* **1994**, *33* (20), 2024–2054.

(5) Shepherd, H. J.; Molnár, G.; Nicolazzi, W.; Salmon, L.; Bousseksou, A. Spin Crossover at the Nanometre Scale. *European Journal of Inorganic Chemistry*. 2013, pp 653–661.

(6) Senthil Kumar, K.; Ruben, M. Emerging Trends in Spin Crossover (SCO) Based Functional Materials and Devices. *Coord. Chem. Rev.* **2017**, *346*, 176–205.

(7) Molnár, G.; Rat, S.; Salmon, L.; Nicolazzi, W.; Bousseksou, A. Spin Crossover Nanomaterials: From Fundamental Concepts to Devices. *Adv. Mater.* **2018**, *30* (5), 1703862.

(8) Mallah, T.; Cavallini, M. Surfaces, Thin Films and Patterning of Spin Crossover Compounds. *Comptes Rendus Chim.* **2018**, DOI:10.1016/j.crci.2018.02.007.

(9) Salmon, L.; Catala, L. 0.1 0.2. *Comptes Rendus Chim.* **2018**, DOI:10.1016/j.crci.2018.07.009.

(10) Trofimenko, S. Boron-Pyrazole Chemistry. IV. Carbon- and Boron-Substituted Poly (1 - Pyrazolyl) Borates. *J. Am. Chem. Soc.* **1967**, *89* (24), 6288–6294.

(11) Rat, S.; Ridier, K.; Vendier, L.; Molnár, G.; Salmon, L.; Bousseksou, A.; Leïchlé, T.; Salmon, L.; Molnár, G.; Bousseksou, A.; et al. Solvatomorphism and Structural-Spin Crossover Property Relationship in Bis[Hydrotris(1,2,4-Triazol-1-Yl)Borate]Iron(Ii). *CrystEngComm* **2017**, *19* (24), 3271–3280.

(12) Ridier, K.; Rat, S.; Shepherd, H. J.; Salmon, L.; Nicolazzi, W.; Molnár, G.; Bousseksou, A. Spatiotemporal Dynamics of the Spin Transition in [Fe (HB (Tz) 3) 2] Single Crystals. *Phys. Rev. B* **2017**, *96* (13), 134106.

(13) Shalabaeva, V.; Rat, S.; Manrique-Juarez, M. D.; Bas, A.-C.; Vendier, L.; Salmon, L.; Molnár, G.; Bousseksou, A.; Claramunt, R. M.; Sanz, D.; et al. Vacuum Deposition of High-Quality Thin Films Displaying Spin Transition near Room Temperature. *J. Mater. Chem. C* **2017**, *5* (18), 4419–4425.

(14) Shalabaeva, V.; Mikolasek, M.; Manrique-Juarez, M. D.; Bas, A.-C.; Rat, S.; Salmon, L.; Nicolazzi, W.; Molnár, G.; Bousseksou, A. Unprecedented Size Effect on the Phase Stability of Molecular Thin Films Displaying a Spin Transition. *J. Phys. Chem. C* **2017**, *121* (45), 25617–25621.

(15) Manrique-Juarez, M. D.; Mathieu, F.; Shalabaeva, V.; Cacheux, J.; Rat, S.; Nicu, L.; Leïchlé, T.; Salmon, L.; Molnár, G.; Bousseksou, A. A Bistable Microelectromechanical System Actuated by Spin-Crossover Molecules. *Angew. Chemie - Int. Ed.* **2017**, *56* (28).

(16) Mikolasek, M.; Manrique-Juarez, M. D.; Shepherd, H. J.; Ridier, K.; Rat, S.; Shalabaeva, V.; Bas, A.-C.; Collings, I. E.; Mathieu, F.; Cacheux, J.; et al. A Complete Set of Elastic Moduli of a Spin-Crossover Solid: Spin-State Dependence and Mechanical Actuation. *J. Am. Chem. Soc.* **2018**, jacs.8b05347.

(17) Shalabaeva, V.; Ridier, K.; Rat, S.; Manrique-Juarez, M. D.; Salmon, L.; Séguy, I.; Rotaru, A.; Molnár, G.; Bousseksou, A. Room Temperature Current Modulation in Large Area Electronic Junctions of Spin Crossover Thin Films. *Appl. Phys. Lett.* **2018**, *112* (1), 013301.

(18) Poggini, L.; Gonidec, M.; González-Estefan, J. H.; Pecastaings, G.; Gobaut, B.; Rosa, P. Vertical Tunnel Junction Embedding a Spin Crossover Molecular Film. *Adv. Electron. Mater.* **2018**, 1800204.

(19) Zhang, J.; Posselt, D.; Sepe, A.; Shen, X.; Perlich, J.; Smilgies, D.-M.; Papadakis, C. M. Structural Evolution of Perpendicular Lamellae in Diblock Copolymer Thin Films during Solvent Vapor Treatment Investigated by Grazing-Incidence Small-Angle X-Ray Scattering. *Macromol. Rapid Commun.* **2013**, *34* (16), 1289–1295.

(20) Jin, C.; Olsen, B. C.; Luber, E. J.; Buriak, J. M. Nanopatterning via Solvent Vapor Annealing of Block Copolymer Thin Films. *Chem. Mater.* **2017**, *29*, 176–188.

(21) Gu, X.; Gunkel, I.; Hexemer, A.; Gu, W.; Russell, T. P. An In Situ Grazing Incidence X-Ray Scattering Study of Block Copolymer Thin Films During Solvent Vapor Annealing. *Adv. Mater.* **2014**, *26* (2), 273–281.

(22) Gu, X.; Gunkel, I.; Hexemer, A.; Russell, T. P. Controlling Domain Spacing and Grain Size in Cylindrical Block Copolymer Thin Films by Means of Thermal and Solvent Vapor Annealing. *Macromolecules* **2016**, *49* (9), 3373–3381.

(23) Nam, S.; Jang, J.; Cha, H.; Hwang, J.; An, T. K.; Park, S.; Park, C. E. Effects of Direct Solvent Exposure on the Nanoscale Morphologies and Electrical Characteristics of PCBM-Based Transistors and Photovoltaics. *J. Mater. Chem.* **2012**, *22* (12), 5543.

(24) Zheng, Y.; Li, S.; Zheng, D.; Yu, J. Effects of Different Polar Solvents for Solvent Vapor Annealing Treatment on the Performance of Polymer Solar Cells. *Org. Electron.* **2014**, *15* (11), 2647–2653.

(25) De Luca, G.; Liscio, A.; Maccagnani, P.; Nolde, F.; Palermo, V.; Müllen, K.; Samorì, P. Nucleation-Governed Reversible Self-Assembly of an Organic Semiconductor at Surfaces: Long-Range Mass Transport Forming Giant Functional Fibers. *Adv. Funct. Mater.* **2007**, *17* (18), 3791–3798.

(26) Wan, L.; Ji, S.; Liu, C.-C.; Craig, G. S. W.; Nealey, P. F. Directed Self-Assembly of Solvent-Vapor-Induced Non-Bulk Block Copolymer Morphologies on Nanopatterned Substrates. *Soft Matter* **2016**, *12* (11), 2914–2922.

(27) Jones, A. O. F.; Geerts, Y. H.; Karpinska, J.; Kennedy, A. R.; Resel, R.; Röthel, C.; Ruzié, C.; Werzer, O.; Sferrazza, M. Substrate-Induced Phase of a [1]Benzothieno[3,2- *b*]Benzothiophene Derivative and Phase Evolution by Aging and Solvent Vapor Annealing. *ACS Appl. Mater. Interfaces* **2015**, *7* (3), 1868–1873.

(28) Ehmann, H. M. A.; Baumgartner, R.; Kunert, B.; Zimmer, A.; Roblegg, E.; Werzer, O. Morphologies of Phenytoin Crystals at Silica Model Surfaces: Vapor Annealing versus Drop Casting. *J. Phys. Chem. C* **2014**, *118* (24), 12855–12861.

(29) Ehmann, H. M. A.; Zimmer, A.; Roblegg, E.; Werzer, O. Morphologies in Solvent-Annealed Clotrimazole Thin Films Explained by Hansen-Solubility Parameters. *Cryst. Growth Des.* **2014**, *14* (3), 1386–1391.

(30) Borgatti, F.; Torelli, P.; Brucale, M.; Gentili, D.; Panaccione, G.; Castan Guerrero, C.; Schäfer, B.; Ruben, M.; Cavallini, M. Opposite Surface and Bulk Solvatochromic Effects in a Molecular Spin-Crossover Compound Revealed by Ambient Pressure X-Ray Absorption Spectroscopy. *Langmuir* **2018**, *34* (12), 3604–3609.

(31) Marcus, Y. The Properties of Organic Liquids That Are Relevant to Their Use as Solvating Solvents. *Chem. Soc. Rev.* **1993**, *22* (6), 409.

(32) Davesne, V.; Gruber, M.; Studniarek, M.; Doh, W. H.; Zafeiratos, S.; Joly, L.; Sirotti, F.; Silly, M. G.; Gaspar, A. B.; Real, J. A.; et al. Hysteresis and Change of Transition Temperature in Thin Films of Fe{[Me2Pyrz]3BH}2, a New Sublimable Spin-Crossover Molecule. *J. Chem. Phys.* **2015**, *142* (19), 194702.

(33) Nam, S.; Chung, D. S.; Jang, J.; Kim, S. H.; Yang, C.; Kwon, S.-K.; Park, C. E. Effects of Poor Solvent for Solution-Processing Passivation of Organic Field Effect Transistors. *J. Electrochem. Soc.* **2010**, *157* (1), H90.